GEOPHYSICS, VOL. 65, NO. 1 (JANUARY-FEBRUARY 2000); P. 232–246, 11 FIGS., 2 TABLES.

Inversion of azimuthally dependent NMO velocity in transversely isotropic media with a tilted axis of symmetry

Vladimir Grechka* and Ilya Tsvankin*

ABSTRACT

Just as the transversely isotropic model with a vertical symmetry axis (VTI media) is typical for describing horizontally layered sediments, transverse isotropy with a tilted symmetry axis (TTI) describes dipping TI layers (such as tilted shale beds near salt domes) or crack systems. P-wave kinematic signatures in TTI media are controlled by the velocity V_{P0} in the symmetry direction, Thomsen's anisotropic coefficients ϵ and δ, and the orientation (tilt ν and azimuth β) of the symmetry axis. Here, we show that all five parameters can be obtained from azimuthally varying P-wave NMO velocities measured for two reflectors with different dips and/or azimuths (one of the reflectors can be horizontal). The shear-wave velocity V_{S0} in the symmetry direction, which has negligible influence on P-wave kinematic signatures, can be found only from the moveout of shear waves.

Using the exact NMO equation, we examine the propagation of errors in observed moveout velocities into estimated values of the anisotropic parameters and establish the necessary conditions for a stable inversion procedure. Since the azimuthal variation of the NMO velocity is elliptical, each reflection event provides us with up to three constraints on the model parameters. Generally, the five parameters responsible for P-wave velocity can be obtained from two P-wave NMO ellipses, but the feasibility of the moveout inversion strongly depends on the tilt ν. If the symmetry axis is close to vertical (small ν), the P-wave NMO ellipse is largely governed by the NMO velocity from a horizontal reflector $V_{\rm nmo}(0)$ and the anellipticity coefficient η. Although for mild tilts the medium parameters cannot be determined separately, the NMO-velocity inversion provides enough information for building TTI models suitable for time processing (NMO, DMO, time migration). If the tilt of the symmetry axis exceeds 30°–40° (e.g., the symmetry axis can be horizontal), it is possible to find all P-wave kinematic parameters and construct the anisotropic model in depth. Another condition required for a stable parameter estimate is that the medium be sufficiently different from elliptical (i.e., ϵ cannot be close to δ). This limitation, however, can be overcome by including the SV-wave NMO ellipse from a horizontal reflector in the inversion procedure.

While most of the analysis is carried out for a single layer, we also extend the inversion algorithm to vertically heterogeneous TTI media above a dipping reflector using the generalized Dix equation. A synthetic example for a strongly anisotropic, stratified TTI medium demonstrates a high accuracy of the inversion (subject to the above limitations).

INTRODUCTION

Transverse isotropy (TI) is a common anisotropic model of the subsurface typical for massive shale formations or thin-bed sedimentary sequences (e.g., Thomsen, 1986). If sediments are horizontally layered, the symmetry axis of the corresponding TI medium is vertical (the so-called VTI model, or vertical transverse isotropy). For dipping TI layers, often found in overthrust areas or near flanks of salt domes and volcanic intrusions, the symmetry axis becomes tilted (TTI media). TI media with a horizontal (HTI) or near-horizontal symmetry axis are often associated with vertical or steeply dipping fracture systems (e.g., Thomsen, 1988).

Reflection traveltime (in general) and NMO velocity (in particular) provide the most reliable information about the anisotropic parameters of TI media. For VTI media, as shown by Alkhalifah and Tsvankin (1995), P-wave NMO velocity in the dip plane of the reflector (and time-domain processing as a

Presented at the 68th Annual Meeting, Society of Exploration Geophysicists. Manuscript received by the Editor June 3, 1998; revised manuscript received February 1, 1999.
*Center for Wave Phenomena, Department of Geophysics, Colorado School of Mines, Golden, CO 80401. E-mail: vgrechka@dix.mines.edu; ilya@dix.mines.edu.

whole) are controlled by only two parameter combinations: the zero-dip NMO velocity (i.e., the NMO velocity for a horizontal reflector)

$$V_{\rm nmo}(0) = V_{P0}\sqrt{1+2\delta} \tag{1}$$

and the anisotropic parameter

$$\eta \equiv \frac{\epsilon-\delta}{1+2\delta}. \tag{2}$$

Here V_{P0} is the P-wave velocity in the symmetry (vertical) direction, and ϵ and δ are Thomsen's (1986) anisotropic coefficients. The values V_{P0}, ϵ, and δ are responsible for all P-wave kinematic signatures in VTI media (Tsvankin, 1996). The parameter η goes to zero in elliptically anisotropic media ($\epsilon = \delta$) and therefore describes the anellipticity of the P-wave slowness surface. (For elliptical anisotropy, NMO velocity is the same function of the ray parameter p and $V_{\rm nmo}(0)$ as in isotropic media.) Provided $V_{\rm nmo}(0)$ has been obtained using semblance analysis of horizontal events, η can be estimated from the NMO velocity for a dipping reflector.

The result of Alkhalifah and Tsvankin (1995) is based on the 2-D NMO equation of Tsvankin (1995) restricted to the dip plane of the reflector. Grechka and Tsvankin (1998) develop a more general 3-D NMO equation valid for common-midpoint (CMP) reflections recorded over arbitrary anisotropic heterogeneous media. They show that the azimuthal variation of NMO velocity is controlled by the spatial derivatives of the ray parameter at the CMP location and usually is described by an ellipse in the horizontal plane. Applying this equation to VTI media, they prove that P-wave NMO velocity is fully governed by $V_{\rm nmo}(0)$ and η for arbitrary orientations of the CMP line and reflector strike. Hence, for VTI media the parameters V_{P0}, ϵ, and δ cannot be resolved individually from P-wave NMO data.

For TI media with a horizontal symmetry axis (HTI), the P-wave kinematic parameters also include the azimuth β of the symmetry axis. (V_{P0} remains the velocity in the symmetry direction, which is horizontal in HTI media, while ϵ and δ are defined with respect to the symmetry axis.) Despite the increase in the number of unknowns, all four moveout parameters can be estimated from azimuthally dependent P-wave NMO velocities measured for a horizontal and dipping reflector (Tsvankin, 1997a; Contreras et al., 1999). Note that P-wave moveout inversion in HTI media provides enough information to perform depth processing, in contrast to time processing in VTI media.

The TI model with a tilted symmetry axis can be considered as intermediate between VTI and HTI. This does not mean, however, that the moveout inversion in TTI media can be understood just by examining the results for the two extreme orientations of the symmetry axis. Indeed, the tilt of the symmetry axis represents an extra parameter to be recovered from moveout data. Tsvankin (1997b) analyzes P-wave NMO velocity in the vertical symmetry plane of TTI media that contain the symmetry axis. To make the problem two dimensional, he also assumes that the symmetry axis is confined to the dip plane of the reflector. He concludes that the NMO velocity is rather sensitive to the tilt ν and depends on ϵ and δ individually (i.e., it is not fully controlled by η for fixed ν). Also, Tsvankin's (1997b) results show that the dip dependence of NMO velocity in the vertical symmetry plane (single azimuth) is not sufficient to resolve the medium parameters.

Here, we carry out a 3-D (azimuthal) analysis of NMO velocity in TI media with arbitrary tilt and azimuth of the symmetry axis. By using the 3-D NMO equation of Grechka and Tsvankin (1998), we develop an inversion procedure to obtain all five relevant parameters (V_{P0}, ϵ, δ, β, and ν) from P-wave NMO ellipses for two reflection events corresponding to different dips. We show that for nonelliptical TI media and the practically important case of a horizontal and a dipping reflector, the inversion procedure becomes stable if reflector dip reaches at least 30° and the tilt of the symmetry axis exceeds 30°–40°. For mild tilts of the symmetry axis, the parameters cannot be resolved individually, but the inversion results are still sufficient to perform time processing. The generalized Dix differentiation (Grechka et al., 1999) allows us to extend the parameter-estimation methodology to vertically heterogeneous TTI media. To estimate the shear-wave velocity V_{S0} in the symmetry direction and increase the overall stability of the inversion procedure, the P-wave moveout can be supplemented with the SV-wave NMO ellipse from a horizontal reflector.

BASIC THEORY OF AZIMUTHALLY VARYING NMO VELOCITY

We start with a brief overview of the analytic representation of NMO velocity in anisotropic media. For moderate offsets x limited by the distance between the CMP and the reflector, reflection moveout t is usually close to a hyperbola (e.g., Taner and Koehler, 1969; Tsvankin and Thomsen, 1994):

$$t^2(x,\alpha) \approx t_0^2 + \frac{x^2}{V_{\rm nmo}^2(\alpha)}, \tag{3}$$

where t_0 is the two-way zero-offset traveltime and $V_{\rm nmo}(\alpha)$ is the NMO velocity, which generally depends on the azimuth α of the CMP line. As shown by Grechka and Tsvankin (1998), NMO velocity of any pure mode can be expressed as

$$V_{\rm nmo}^{-2}(\alpha) = W_{11}\cos^2\alpha + 2\,W_{12}\sin\alpha\cos\alpha + W_{22}\sin^2\alpha, \tag{4}$$

where $W_{ij} = \tau_0\,\partial p_i/\partial x_j$ $(i, j = 1, 2)$, $\tau_0 = t_0/2$ are the one-way zero-offset traveltime, p_i are the horizontal components of the slowness vector for one-way rays emanating from the zero-offset reflection point, and x_i are the horizontal spatial coordinates. The derivatives are evaluated at the CMP. (For brevity, we will not show the azimuth α explicitly as an argument of the NMO-velocity function; the value of α in each case will be clear from the context.)

Equation (4) is valid for pure modes in arbitrary anisotropic heterogeneous media as long as the reflection traveltime can be expanded in a Taylor series in x_i near the CMP location. Unless reflection traveltime decreases with offset in a certain direction leading to so-called reverse moveout [i.e., there is at least one azimuth α for which $V_{\rm nmo}^2(\alpha) < 0$], the symmetric matrix $\mathbf{W}$ is positive definite and equation (4) describes an ellipse. Clearly, the NMO ellipse is fully determined by the three elements of the matrix $\mathbf{W}$.

For a homogeneous anisotropic layer above a dipping reflector, the matrix $\mathbf{W}$ becomes the following function of the

slowness components p_i (Grechka et al., 1999):

$$\mathbf{W} = \frac{p_1 q_{,1} + p_2 q_{,2} - q}{q_{,11} q_{,22} - q_{,12}^2} \begin{pmatrix} q_{,22} & -q_{,12} \\ -q_{,12} & q_{,11} \end{pmatrix}, \qquad (5)$$

where $q \equiv q(p_1, p_2) \equiv p_3$ denotes the vertical component of the slowness vector, $q_{,i} \equiv \partial q / \partial p_i$, and $q_{,ij} \equiv \partial^2 q / \partial p_i \partial p_j$. The horizontal slowness components p_1 and p_2 and all derivatives are evaluated for the zero-offset ray.

Note that p_1 and p_2 control the reflection slope on the zero-offset (stacked) section and therefore can be obtained directly from reflection data. The vertical slowness $q = q(p_1, p_2)$ in a known anisotropic model can be found by solving the Christoffel equation for given values of p_1 and p_2. Then, implicit differentiation of Christoffel equation yields the derivatives $q_{,i}$ and $q_{,ij}$ (Grechka et al., 1999). Therefore, equation (5) provides a simple and numerically efficient recipe for obtaining NMO velocity of pure modes in a layer with any anisotropic symmetry.

SPECIAL CASES OF TTI MEDIA

Appendix A discusses NMO velocity for three different types of tilted TI models that require special treatment: (1) TTI medium above a steep reflector, (2) tilted elliptically anisotropic medium, and (3) TI medium with the symmetry axis perpendicular to the reflector (model typical for overthrust areas).

In all three cases, NMO velocity has certain distinct features that need to be taken into account in the inversion procedure. For instance, the P-wave NMO ellipse in a single TI layer with the symmetry axis orthogonal to the reflector is governed by the symmetry-direction velocity V_{P0} and the parameter δ and is independent of another anisotropic parameter, ϵ.

Below, we provide a detailed analysis of the P-wave NMO velocity in TTI media with weak anisotropy (i.e., with small values of $|\epsilon|$ and $|\delta|$).

Weakly anisotropic horizontal layer

Although equations (4) and (5) give a concise representation of azimuthally varying NMO velocity, the dependence of $V_{\rm nmo}$ on the model parameters is hidden in the components of the slowness vector. To understand the influence of the axis orientation and anisotropic parameters on the P-wave NMO velocity, we linearize equation (5) with respect to ϵ and δ assuming that $|\epsilon| \ll 1$ and $|\delta| \ll 1$ (Appendix B). The final expressions (B-7) and (B-8) are given for the coordinate system in which the azimuth of the symmetry axis $\beta = 0$ (i.e., the symmetry axis is in the $[x_1, x_3]$-plane; see Figure B-1). Note that the shear-wave velocity in the symmetry direction (V_{S0}) does not appear in the linearized NMO equations because all P-wave kinematic signatures in the weak-anisotropy approximation are independent of V_{S0} (Tsvankin, 1996).

For a horizontal reflector ($p_1 = p_2 = 0$) equations (B-7) and (B-8) can be simplified to

$$W_{11} = \frac{1}{V_{P0}^2} \left[1 - 2\delta + 2\epsilon \sin^2 \nu - 14 (\epsilon - \delta) \sin^2 \nu \cos^2 \nu\right], \qquad (6)$$

$$W_{12} = 0, \qquad (7)$$

$$W_{22} = \frac{1}{V_{P0}^2} \left[1 - 2\delta - 2 (\epsilon - \delta) \sin^2 \nu (1 + \cos^2 \nu)\right]. \qquad (8)$$

Since $W_{12} = 0$, the semiaxes of the P-wave NMO ellipse for a horizontal reflector are parallel to the coordinate axes x_1 and x_2. This result could be expected because the $[x_1, x_3]$-plane contains the symmetry axis and therefore represents a symmetry plane of the horizontal TTI layer. In the case of vanishing W_{12}, the quantities W_{11} and W_{22} are reciprocal to the squared NMO velocities along the axes of the ellipse (Grechka and Tsvankin, 1998):

$$W_{ii} = \frac{1}{\left[V_{\rm nmo}^{(i)}(0)\right]^2}, \qquad (i = 1, 2). \qquad (9)$$

The velocity $V_{\rm nmo}^{(1)}(0)$ corresponds to the CMP line in the vertical plane that contains the symmetry axis. Equations (6) and (9) for $V_{\rm nmo}^{(1)}(0)$ are equivalent to the result of Tsvankin (1997b) [his equation (23)], who studies NMO only in this vertical symmetry plane. Equations (6)–(8) provide us with three constraints on the layer parameters: the orientation of the NMO ellipse depends on the azimuth β of the symmetry axis, while the values of the semiaxes give two more equations for all five parameters. Note that the azimuth of the symmetry axis cannot be unambiguously found from the NMO ellipse from a horizontal reflector because β can be equal to the azimuth of either semimajor or semiminor axis, depending on the medium parameters. For HTI media ($\nu = 90^\circ$) resulting from parallel penny-shaped cracks, the symmetry axis coincides with the semimajor axis of the ellipse (Tsvankin, 1997a).

The number of equations, however, reduces to two if the NMO ellipse degenerates into a circle, i.e.,

$$V_{\rm nmo}^{(1)}(0) = V_{\rm nmo}^{(2)}(0). \qquad (10)$$

Obviously, for VTI media ($\nu = 0$) NMO velocity is always independent of azimuth and $V_{\rm nmo}^{(1)}(0) = V_{\rm nmo}^{(2)}(0) = V_{\rm nmo}(0) = V_{P0}\sqrt{1 + 2\delta}$ [equation (1)]. Interestingly, condition (10) can also be satisfied for azimuthally anisotropic media with a tilted symmetry axis. Substituting equations (6), (8), and (9) into equation (10) and assuming $\nu \neq 0$, we find

$$2\epsilon - \delta - 6 (\epsilon - \delta) \cos^2 \nu = 0. \qquad (11)$$

For instance, if the symmetry axis is horizontal ($\cos \nu = 0$), relation (11) gives

$$2\epsilon - \delta = 0, \qquad (12)$$

which represents a known condition for the P-wave NMO ellipse in weakly anisotropic HTI media to degenerate into a circle. The ellipticity of P-wave NMO velocity in HTI media is governed by the coefficient $\delta^{(V)} \approx 2\epsilon - \delta$ (Tsvankin, 1997a), which goes to zero if equation (12) is satisfied.

An example of azimuthally independent NMO velocity for TI media with a tilt angle of 45° is shown in Figure 1. Equation (11) with $\nu = 45^\circ$ yields $\epsilon - 2\delta = 0$; so for the model from Figure 1, the semiaxes of the NMO ellipse should be equal to each other. Although equation (11) is an approximation valid only for weakly anisotropic media, the exact NMO ellipse calculated using equation (5) is indeed almost circular.

Another important point illustrated by Figure 1 is that the theoretical NMO ellipse (solid) is close to the ellipse

reconstructed from ray-traced traveltimes for spread length equal to the reflector depth (dotted). The difference between the two ellipses, caused by the deviation of the moveout curve from the analytic hyperbola, is limited by 1.1%. This example and other numerical tests we performed show that for moderately anisotropic TTI media the influence of nonhyperbolic moveout on P-wave moveout velocity can be ignored as long as the maximum offset does not exceed reflector depth. The same conclusion is drawn by Tsvankin (1997b) in his study of the 2-D moveout problem in TTI media.

Weakly anisotropic dipping layer

The P-wave NMO ellipse from a horizontal reflector provides either two or three constraints on the parameters of the TTI layer, depending on whether the ellipse degenerates into a circle. To resolve all five relevant layer parameters ($V_{P0}, \epsilon, \delta, \beta$, and ν), we suggest including the NMO ellipse from a dipping reflector (i.e., three more equations) in the inversion procedure.

Although there seem to be enough equations to recover all unknowns, in certain situations the parameters cannot be resolved individually. The weak-anisotropy approximation of the P-wave NMO ellipse [equations (B-7) and (B-8)] helps us to identify the trade-offs between model parameters and study the stability of the inversion procedure. For instance, equation (B-7) shows that the anisotropic coefficients in all dip-dependent terms appear only as the difference $\epsilon - \delta$; indeed, for elliptical anisotropy ($\epsilon = \delta$) the dip dependence of NMO velocity is purely isotropic (Appendix A). Still, ϵ and δ can be resolved individually using the NMO ellipse for horizontal events [equations (6) and (8)], unless the tilt ν is relatively small (estimates are given in the next section). For small values of ν, the medium approaches VTI and the NMO velocity from a horizontal reflector yields a single quantity ($V_{P0}\sqrt{1+2\delta}$), while the dip dependence of NMO velocity is controlled by $\eta \approx \epsilon - \delta$ (Alkhalifah and Tsvankin, 1995). Thus, ϵ and δ can be estimated separately, but only for a sufficiently large tilt of the symmetry axis.

A similar constraint applies to the reflector dip, which should not be too mild for the dip dependence of NMO velocity to be sensitive enough to the anisotropic parameters. [The anisotropic dip terms $\hat{W}_{ij}$ in the weak-anisotropy approximation (B-8) can be used to make appropriate estimates.] On the whole, determination of the five relevant parameters of TTI media from the P-wave NMO ellipses for a horizontal and a dipping reflector should be feasible if both the reflector dip and the tilt of the symmetry axis are not too small. In the next section, we quantify this statement by performing the actual inversion based on the exact NMO equation.

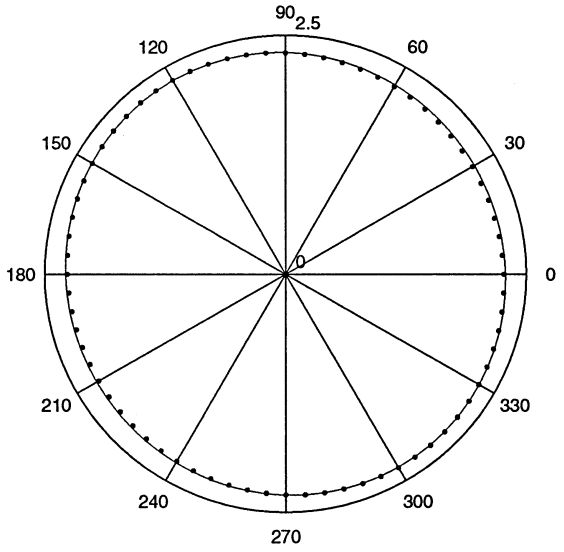

FIG. 1. Quasi-circular P-wave NMO ellipses in a horizontal TTI layer. Solid inner curve—the ellipse computed using equation (5). Dotted curve—the best-fit ellipse reconstructed using the hyperbolic equation (3) from ray-traced traveltimes computed along four CMP lines at azimuths 0°, 45°, 90°, and 135° (the azimuth is shown around the plot). Spreadlength is equal to the thickness of the layer. The relevant medium parameters are $V_{P0} = 2.0$ km/s, $\epsilon = 0.2$, $\delta = 0.1$, $\beta = 30°$, and $\nu = 45°$. The value 2.5 at the top of the plot indicates the range of NMO velocity in km/s.

PARAMETER ESTIMATION IN A TTI LAYER USING *P*-WAVES

Inversion algorithm

The P-wave NMO ellipses for a horizontal [$\tilde{\mathbf{W}}^{\rm hor}$ or $\tilde{V}^{\rm hor}_{\rm nmo}(\alpha)$] and a dipping [$\tilde{\mathbf{W}}^{\rm dip}$ or $\tilde{V}^{\rm dip}_{\rm nmo}(\alpha)$] event in a homogeneous TTI layer (input data) can be inverted for five medium parameters: $V_{P0}, \epsilon, \delta, \nu$, and β. We obtain the parameters by minimizing the least-squares objective function

$$\mathcal{F}_P = \int_0^{2\pi} \left[1 - \frac{V^{\rm hor}_{\rm nmo}(\alpha)}{\tilde{V}^{\rm hor}_{\rm nmo}(\alpha)}\right]^2 d\alpha + \int_0^{2\pi} \left[1 - \frac{V^{\rm dip}_{\rm nmo}(\alpha)}{\tilde{V}^{\rm dip}_{\rm nmo}(\alpha)}\right]^2 d\alpha, \qquad (13)$$

where the NMO velocities $V^{\rm hor}_{\rm nmo}(\alpha)$ and $V^{\rm dip}_{\rm nmo}(\alpha)$ are calculated using the exact equation (5) for a particular model. The objective function was minimized using the simplex method. Although in principle the nonlinear system (13) might have multiple solutions, extensive numerical testing shows that for error-free input data and a realistic starting model (i.e., $|\epsilon| < 1$, $|\delta| < 1$) the inversion algorithm always converges toward the correct set of parameters.

Influence of tilt on inversion results

For numerical testing, we computed the matrices $\tilde{\mathbf{W}}^{\rm hor}$ and $\tilde{\mathbf{W}}^{\rm dip}$ from equation (5) and built the corresponding NMO ellipses. To simulate inaccuracies in velocity picking, we introduced errors into the NMO velocities in four azimuthal directions (0°, 45°, 90°, and 135°) by adding Gaussian noise with a variance of 2%. Then we obtained the ellipses that provide the best approximation for the new (distorted) NMO velocities and carried out the inversion using equation (13).

Figure 2 shows the results of parameter estimation for TTI layers with different tilts ν of the symmetry axis. Each dot on the plots corresponds to the inversion result for a particular realization of errors in the NMO ellipses; the inversion procedure for each model was repeated 200 times. The mean values of all

parameters were recovered accurately despite the fact that we intentionally used an incorrect shear-wave velocity $V_{S0} = V_{P0}/2$ to perform the inversion. Hence, in agreement with the results of Tsvankin (1996, 1997b) and the weak-anisotropy approximations (B-7) and (B-8), V_{S0} has a negligible influence on P-wave moveout in TI media.

Figure 2 also confirms that the inversion becomes more stable with increasing tilt of the symmetry axis. While the inverted parameters ϵ and δ are tightly clustered near the actual values for the tilts $\nu = 60^\circ$ and $\nu = 80^\circ$, the deviations visibly increase for $\nu = 40^\circ$ (Figure 2c) and especially for $\nu = 20^\circ$ (Figure 2a). The inversion results for $\nu < 30^\circ$–40° are so sensitive to errors in the input parameters that P-wave NMO velocity cannot be used to resolve ϵ and δ individually. Nonetheless, the inverted values of ϵ and δ show a linear trend described by the line corresponding to the correct value of η [see equation (2)]. For VTI media ($\nu = 0$), η is the only combination of the anisotropic parameters constrained by the P-wave NMO velocity (Alkhalifah and Tsvankin, 1995).

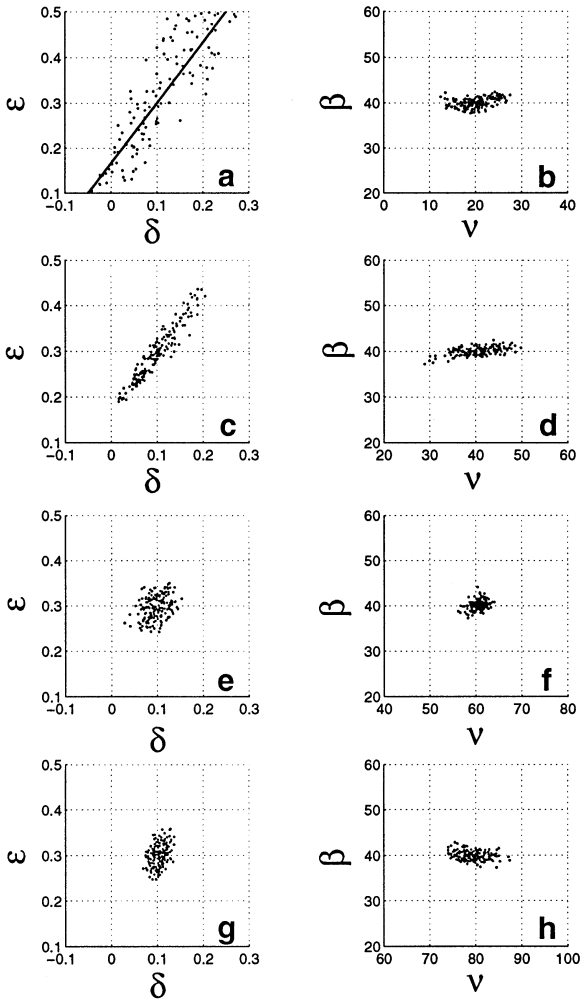

FIG. 2. Inverted values of the parameters ϵ, δ, β, and ν in a homogeneous TTI layer. As the input data we use the P-wave NMO ellipses from a horizontal and a dipping reflector (dip $\phi = 60^\circ$; azimuth $= 50^\circ$). Both ellipses were distorted by random noise with a variance of 2%. The actual values are $V_{P0} = 2.0$ km/s, $V_{S0} = 1.2$ km/s, $\epsilon = 0.3$, $\delta = 0.1$, $\beta = 40^\circ$. The tilt ν is equal to 20° in (a) and (b), 40° in (c) and (d), 60° in (e) and (f), and 80° in (g) and (h). The solid line on plot (a) indicates values of ϵ and δ corresponding to the correct value of $\eta = 0.167$.

The accuracy in the P-wave symmetry-direction velocity V_{P0} (not shown in Figure 2) exhibits a similar dependence on the tilt, with the scatter in the inversion results monotonically increasing with decreasing ν. The standard deviation in V_{P0} changes from a small value of 0.01 km/s (0.5% of the correct V_{P0}) for a near-horizontal symmetry axis ($\nu = 80^\circ$) to 0.26 km/s (13%) for a tilt of 20°. For a near-vertical symmetry axis, P-wave NMO can be used to obtain the zero-dip NMO velocity ($V_{P0}\sqrt{1+2\delta}$) but not V_{P0} or δ separately (see the analysis for VTI media in Alkhalifah and Tsvankin, 1995).

Another interesting observation, this time from the right-column plots in Figure 2, is that the azimuth β of the symmetry axis is well constrained for all four tilts ν, while the scatter in the tilt itself is more significant. Overall, the accuracy in both β and ν is quite satisfactory for a wide range of tilts; an exception is quasi-VTI models with small $\nu < 10^\circ$ (not shown) for which the orientation of the symmetry axis does not have much influence on NMO velocity. Also, the scatter in the azimuth and tilt of the symmetry axis increase as the medium approaches isotropic ($|\epsilon| < 0.05$, $|\delta| < 0.05$) because all kinematic signatures in this case lose their sensitivity to the symmetry-axis direction.

Time processing for mild tilts

The stability analysis indicates that the parameters responsible for P-wave kinematics cannot be resolved unambiguously for a relatively wide range of mild tilts of the symmetry axis ($\nu < 30^\circ$–40°). Hence, an important practical question is whether moveout inversion for mild ν provides any useful information for seismic processing.

As mentioned above, if the medium has the VTI symmetry ($\nu = 0$), P-wave moveout data constrain two parameter combinations [$V_{\rm nmo}(0)$ and η], which are fully responsible for all time-processing steps (NMO, DMO, and time migration). For TTI models with a mild tilt ν, our algorithm produces a family of equivalent models, all of which have close NMO ellipses for the two reflectors used in the inversion. To verify whether these equivalent models can replace the actual model in time processing, we computed nonhyperbolic moveout from a horizontal reflector and NMO ellipses from dipping reflectors for a representative subset of models obtained in Figures 2a,b. A typical result, displayed in Figure 3, demonstrates that the long-spread (nonhyperbolic) moveout curves for the actual model and a substantially different set of the inverted parameters are indeed close to each other in all azimuthal directions. We conclude that these two models have similar impulse responses for poststack time migration.

NMO ellipses for equivalent models (not shown here) almost coincide for reflectors with the azimuth used in the inversion but somewhat diverge from each other with increasing dip if the reflector has a different orientation. Still, for practical purposes of DMO processing, it should be acceptable to use a model found from NMO velocity inversion, especially if the subsurface structure does not contain a wide range of reflector azimuths. Therefore, although the moveout-inversion

algorithm cannot resolve the medium parameters for mild tilts of the symmetry axis, it allows us to build an approximate TTI model for time-domain processing.

Influence of reflector dip

The inversion results in Figure 2 were obtained for a rather favorable (large) reflector dip $\phi = 60^\circ$. As expected, the inversion becomes less stable as the dipping reflector tilts toward horizontal (Figure 4). Each row of plots in Figure 4 should be compared with Figures 2e,f, which were generated for the same $\nu = 60^\circ$. While the scatter in the inverted parameters for the dips $\phi = 40^\circ$ (Figures 4e,f) and $\phi = 60^\circ$ (Figures 2e,f) is comparable, the results deteriorate for a smaller $\phi = 30^\circ$ (Figures 4c,d) and become quite unstable for $\phi = 20^\circ$ (Figures 4a,b). The inverted values of ϵ and δ in Figure 4a still cluster around a straight line, but this line is no longer described by the actual parameter η. Note that the scatter in the parameters responsible for the symmetry-axis orientation is much more sensitive to the reflector dip (the right column of plots in Figure 4) than to the tilt of the axis (Figure 2). The standard deviation in the symmetry-direction velocity V_{P0} (not shown) also increases from 1.2% for $\phi = 40^\circ$ to 3.1% for $\phi = 30^\circ$ to 6.8% for $\phi = 20^\circ$.

Therefore, the dip should reach at least 30° for the inversion to be reasonably stable. Similar values of the minimum dip were given by Alkhalifah and Tsvankin (1995), who used the dip dependence of NMO velocity in the inversion for the anisotropic parameter η in VTI media. On the other hand, the reflector should not be too steep either because, for dips approaching 90°, specular reflections and the NMO ellipse may not exist at all (see Appendix A).

We conclude that the moveout inversion based on the P-wave NMO ellipses for a horizontal and a dipping reflector yields sufficiently stable results if both the reflector dip ϕ and tilt of the axis ν exceed 30°–40°.

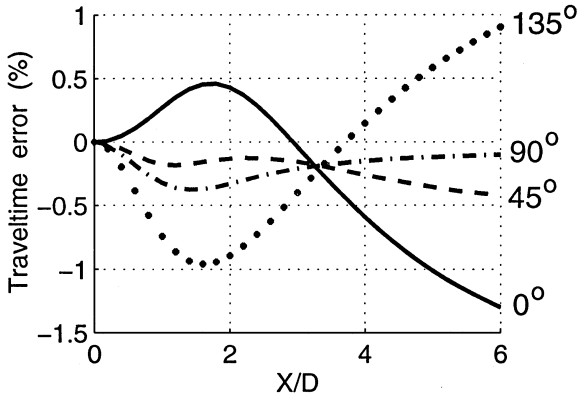

FIG. 3. Comparison of long-spread reflection moveout from a horizontal interface for the actual TTI model and an equivalent model obtained by NMO-velocity inversion. The curves, computed for several azimuthal directions marked on the plot, show the difference between the reflection traveltimes for the two models as a function of the offset X normalized by the reflector depth D. The parameters of the actual model (taken from Figures 2a,b) are $V_{P0} = 2.0$ km/s, $\epsilon = 0.3$, $\delta = 0.1$, $\nu = 20^\circ$, $\beta = 40^\circ$; for the equivalent model, $V_{P0} = 2.2$ km/s, $\epsilon = 0.14$, $\delta = 0.03$, $\nu = 21.5^\circ$, $\beta = 40.8^\circ$.

Inversion for elliptical anisotropy

In addition to the constraints on ν and ϕ, stable moveout inversion requires that the parameters ϵ and δ be sufficiently different from one another. If $\epsilon = \delta$ (the medium is elliptical), the dip dependence of the P-wave NMO velocity is purely isotropic [equation (A-4)] and the only information contained in the NMO ellipse for the dipping event is that $\epsilon = \delta$. This implies that a single P-wave NMO ellipse for a horizontal event (three equations) has to be used to recover the four remaining parameters (V_{P0}, ϵ, ν, and β). Obviously, this inversion is ambiguous, and it is possible to find a family of elliptical models with identical NMO ellipses from horizontal and dipping reflectors (Figure 5). To overcome the ambiguity, we need to know one of the parameters beforehand. For instance, if the symmetry axis is assumed to be horizontal ($\nu = 90^\circ$; HTI media), the remaining three parameters can be obtained from the NMO ellipse for horizontal events.

In Appendix C we show that the parameters of elliptical media can be resolved for arbitrary orientation of the symmetry axis if P-wave moveout data are supplemented with the SV-wave NMO velocity from a horizontal reflector. The addition of shear data also helps to increase the stability of the inversion procedure and evaluate the S-wave symmetry-direction velocity V_{S0}.

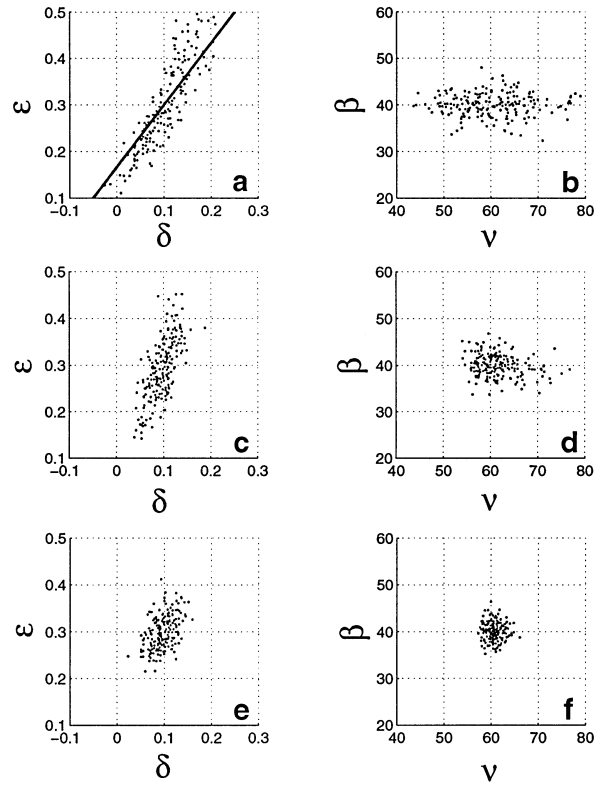

FIG. 4. Same as Figure 2, but for variable reflector dip. The parameters V_{P0}, ϵ, δ, β, and the reflector azimuth are the same as those in Figure 2; the tilt of the symmetry axis $\nu = 60^\circ$. The reflector dip $\phi = 20^\circ$ in (a) and (b), 30° in (c) and (d), and 40° in (e) and (f). The solid line on plot (a) corresponds to the correct value of $\eta = 0.167$.

P-WAVE MOVEOUT INVERSION IN VERTICALLY HETEROGENEOUS TTI MEDIA

The above discussion was limited to moveout inversion for a single homogeneous TTI layer. Here, we extend the parameter estimation methodology to vertically heterogeneous TTI media composed of a stack of horizontal TTI layers (the orientation of the symmetry axis may be arbitrary) above a dipping reflector.

Azimuthally varying NMO velocity for this model can be expressed through the interval NMO ellipses using the generalized Dix equation of Grechka et al. (1999). The interval NMO ellipse $\mathbf{W}_\ell$ in layer ℓ can be found by means of the Dix-type differentiation

$$\mathbf{W}_\ell^{-1} = \frac{\tau(\ell)\mathbf{W}^{-1}(\ell) - \tau(\ell-1)\mathbf{W}^{-1}(\ell-1)}{\tau(\ell) - \tau(\ell-1)}, \qquad (14)$$

where $\mathbf{W}(\ell-1)$ and $\mathbf{W}(\ell)$ describe the NMO ellipses for the reflections from the top and bottom of the layer and $\tau(\ell-1)$ and $\tau(\ell)$ are the corresponding zero-offset traveltimes. Although this equation looks similar to the well-known Dix (1955) formula (one may think about formally replacing the matrices $\mathbf{W}^{-1}$ by the squared NMO velocities), it is much more general because it fully accounts for the simultaneous influence of arbitrary anisotropy and reflector dip on the azimuthally dependent NMO velocity. Equation (14) is not restricted to any particular anisotropic symmetry and can be used for all pure reflected modes (*P*- or *S*-waves). For example, Grechka and Tsvankin (1999) apply this equation to moveout inversion of *P*-wave data in vertically heterogeneous orthorhombic media.

The effective and interval NMO ellipses in equation (14) are evaluated for the slowness components of the zero-offset ray. In the case of horizontal events, the zero-offset slowness vector is vertical for all reflections (i.e., its horizontal components vanish), and the interval ellipse can be found directly from the effective ellipses for the reflections from the top and bottom of the layer. For dipping reflectors, however, the ray parameters of the zero-offset ray change from one reflection event to another, depending on the reflector dip and elastic parameters in a particular layer. Therefore, after carrying out the inversion in the subsurface layer using the technique described in the previous sections, we need to calculate the matrix $\mathbf{W}$ in this layer for the slowness components of the zero-offset reflection from the dipping interface in the second layer. Then we obtain the interval NMO ellipse for the dipping event in the second layer from equation (14), combine it with the corresponding ellipse from the horizontal reflector, carry out the inversion in the second layer, and continue the layer-stripping procedure downward.

We applied our inversion algorithm to synthetic data generated for a three-layer TTI model with a dipping reflector (e.g., a fault plane) shown in Figure 6. Note that the azimuth β of the symmetry axis varies from layer to layer (Table 1), so the model does not have a throughgoing vertical symmetry plane. We performed 3-D anisotropic ray tracing and computed *P*-wave reflection traveltimes from the horizontal and dipping reflectors along four CMP lines at azimuths 0°, 45°, 90°, and 135° with respect to the orientation of the dipping reflector. Then we fit hyperbolas [equation (3)] to the computed traveltimes on conventional-length spreads and obtained azimuthally varying effective moveout velocities. After approximating these velocities by the best-fit NMO ellipses [equation (4)], we used the generalized Dix formula [equation (14)] to calculate the interval ellipses (as described above) and carried out parameter estimation in each layer.

The inversion results are shown in Table 2. Since *SV*-wave reflections were not used in this test, we could not obtain the

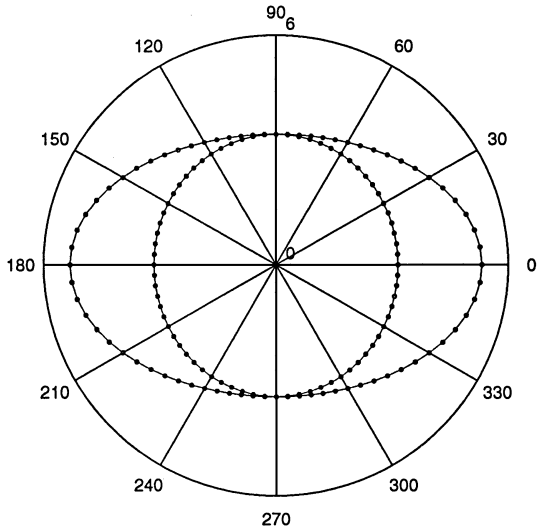

FIG. 5. *P*-wave NMO ellipses for horizontal and dipping reflectors calculated from the exact equation (5) in an elliptical TTI layer for two different sets of medium parameters. The solid ellipses are computed for $V_{P0} = 3.0$ km/s, $\epsilon = \delta = 0.15$, and $\nu = 50°$; for the dipping reflector, $\phi = 50°$. For the dotted ellipses, $V_{P0} = 2.44$ km/s, $\epsilon = \delta = 0.48$, $\nu = 25°$, $\phi = 40°$. The azimuth of the symmetry axis and that of the dipping reflector equal zero for both models.

Table 1. Actual values of the interval parameters for the model in Figure 6.

Layer	V_{P0} (km/s)	V_{S0} (km/s)	ϵ	δ	ν (°)	β (°)
1	2.00	1.20	0.15	0.10	50.0	20.0
2	2.50	1.60	0.20	0.10	60.0	40.0
3	3.00	1.80	0.30	0.15	40.0	60.0

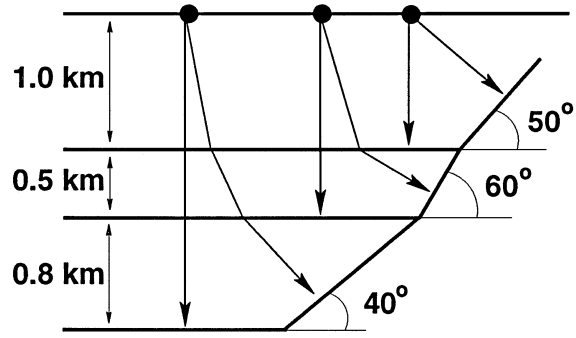

FIG. 6. A 2-D sketch of the layered TTI model used to test the inversion algorithm. The azimuth of the reflector is 0°; layer thicknesses and reflector dips ϕ in each interval are shown on the plot. Layer parameters are given in Table 1.

shear-wave symmetry-direction velocity V_{S0}. The errors in the medium parameters for all layers are rather small and mostly result from the influence of nonhyperbolic moveout on the finite-spread moveout velocity. Although we used an incorrect (best-guess) value of V_{S0} by assuming $V_{S0} = V_{P0}/2$, V_{S0} has a practically negligible influence on P-wave moveout. To verify this conclusion again, we carried out the inversion for the third layer using the exact NMO ellipses [given by equation (5)], rather than the ones obtained from the ray-traced traveltimes, and an incorrect $V_{S0} = 1.5$ km/s. The inversion result in this case was almost perfect: $V_{P0} = 2.98$ km/s, $\epsilon = 0.31$, $\delta = 0.16$, $\nu = 39.8^\circ$, and $\beta = 60.3^\circ$ (compare to the last lines in Tables 1 and 2).

Nonhyperbolic moveout, caused by both vertical heterogeneity and anisotropy, introduces distortions into the moveout velocity, which propagate into the interval NMO ellipses after being amplified by the Dix differentiation [equation (14)]. [Note that the azimuthal variation of the fourth-order (quartic) moveout term is not an ellipse; in a horizontal layer, it is described by a quartic oval curve (Sayers and Ebrom, 1997).] The maximum deviations of the interval NMO velocities from the exact ellipses, however, are quite moderate [0.5%, 3.0%, and 1.9% for the first (subsurface), second, and third layers, respectively] and correspond to the horizontal events. Hence, it is justified to use the hyperbolic moveout approximation for P-waves on conventional spread lengths close to the distance between CMP and reflector.

Although the largest error in the NMO velocity (3.0%) was observed in the second layer, the inversion results are least accurate for the bottom (third) layer (see Table 2). This is explained by the larger tilt ν of the symmetry axis in the second layer (60° compared to 40° in the third layer), which makes the inverted parameters less sensitive to errors in the input data. Indeed, the scatter of the inversion results in Figures 2c–f is noticeably smaller for the tilt $\nu = 60^\circ$ than that for $\nu = 40^\circ$.

Overall, the accuracy of the inversion in vertically heterogeneous TTI media can be predicted on the basis of the single-layer error analysis with a correction that accounts for the amplification of errors inherent in the Dix-type layer stripping.

DISCUSSION AND CONCLUSIONS

We showed that the NMO ellipses of reflection events obtained from 3-D (azimuthal) moveout analysis can be used to determine the parameters of layered TTI media. For P-waves, reflection moveout and all other kinematic signatures in TTI media depend on five parameters: the symmetry-direction P-wave velocity V_{P0}, anisotropic coefficients ϵ and δ, and the orientation (tilt ν and azimuth β) of the symmetry axis. Since each NMO ellipse provides us with up to three equations for the medium parameters, the inversion procedure requires at least two ellipses for different reflection events. By developing the weak-anisotropy approximation and performing numerical inversion based on the exact NMO equation, we showed the feasibility of parameter estimation for the most common case of a horizontal and a dipping reflector. The parameters V_{P0}, ϵ, δ, ν, and β are sufficient to perform P-wave depth processing in TTI media.

Stable inversion for all parameters, however, is impossible unless the model satisfies several constraints listed below.

Table 2. Inverted interval parameters for the model from Figure 6. The maximum source-receiver offset used in estimating moveout velocities is equal to the distance between the CMP and the corresponding reflector. Compare with the actual values from Table 1.

Layer	V_{P0} (km/s)	ϵ	δ	ν ($^\circ$)	β ($^\circ$)
1	2.02	0.14	0.09	53.6	19.6
2	2.52	0.19	0.10	60.1	38.9
3	2.91	0.38	0.14	43.7	64.5

The tilt ν of the symmetry axis should be greater than 30°–40°.—For VTI media ($\nu = 0$), P-wave reflection moveout depends on just two combinations of medium parameters: the zero-dip NMO velocity and the anisotropic coefficient η close to the difference between ϵ and δ (Alkhalifah and Tsvankin, 1995; Grechka and Tsvankin, 1998). Therefore, it is not surprising that the P-wave NMO ellipses become insensitive to the individual values of V_{P0}, ϵ, and δ for relatively mild tilts of the symmetry axis. Our numerical results show that if ν is less than 30°–40°, the dip dependence of NMO velocity allows us to estimate only a combination of ϵ and δ that becomes close to η with decreasing tilt. Nevertheless, although the individual parameters for mild tilts cannot be resolved, all models obtained from the NMO-velocity inversion provide an acceptable approximation for time-domain processing (NMO, DMO, and time migration).

Reflector dip ϕ should be >30° but <80°.—If the dip is below 30°, the dip-dependent terms are not large enough for the anisotropic inversion. A similar minimum dip requirement in the P-wave moveout inversion was obtained for VTI media by Alkhalifah and Tsvankin (1995) and for HTI media by Contreras et al. (1999). Although the inversion becomes more stable with increasing dip, specular reflections in a homogeneous medium may not exist at all for dips approaching 80° (see Appendix A).

The medium cannot be close to elliptical.—If the difference between ϵ and δ is small, the medium approaches elliptical anisotropy ($\epsilon = \delta$), and the moveout data can provide only the NMO ellipse for horizontal events and an estimate of $\epsilon - \delta$.

The inversion procedure assumes that the tilt of the symmetry axis does not vary with reflector dip.—This assumption, however, may be violated in models typical for overthrust areas (such as the Canadian Foothills) where the symmetry axis often remains perpendicular to the reflector. In this important special case, as shown in Appendix A, P-wave NMO velocity in a single TTI layer can be inverted for the symmetry-direction velocity V_{P0} and the parameter δ. To determine the second anisotropic parameter, ϵ, it is necessary to use reflections from deeper (e.g., horizontal) interfaces beneath the dipping TTI layer.

If multicomponent data are recorded, the stability of the parameter estimation can be enhanced by including NMO velocities of shear waves into the inversion procedure. The addition of the SV-wave NMO ellipse from a horizontal reflector helps to increase the accuracy of the inversion since the SV-wave moveout depends on only one exrtra parameter (the symmetry-direction shear velocity V_{S0}). Also, combining SV

reflections from a horizontal interface with the P-wave NMO ellipses for a horizontal and a dipping reflector makes it possible to determine the parameters of elliptically anisotropic media. Still, including horizontal SV events is not sufficient to overcome the above constraints on the tilt of the symmetry axis and reflector dip (conditions 1 and 2 above).

Extension of our inversion scheme to vertically heterogeneous TTI media is based on the generalized Dix equation (Grechka et al., 1999), which expresses the NMO velocity through the matrices responsible for the interval NMO ellipses. As a result of the Dix-type layer stripping, we obtain the interval NMO velocity, which can be inverted for the medium parameters using the single-layer algorithm. This inversion methodology was tested successfully on a synthetic data set generated by 3-D anisotropic ray tracing in a multilayered TTI model with depth-varying azimuth and tilt of the symmetry axis. General results for a single layer hold in stratified media as well, with additional restrictions imposed by layer stripping (e.g., the layer of interest must be sufficiently thick).

The TTI model discussed here should be rather common in overthrust regions and near salt domes. Our inversion methodology provides an efficient way of estimating the anisotropic parameters that may be needed for seismic imaging in these important exploration areas (Leslie and Lawton, 1996; Vestrum et al., 1999).

ACKNOWLEDGMENTS

We thank Ken Larner (CSM) and Phil Anno (Conoco) for helpful discussions. We are also grateful to Ken Larner, Associate Editor Ali Tura (Chevron), and Joe Dellinger (BP/Amoco) for their reviews of the manuscript. The support for this work was provided by the members of the Consortium Project on Seismic Inverse Methods for Complex Structures at the Center for Wave Phenomena, Colorado School of Mines, and by the U.S. Department of Energy. I.T. was also supported by the Shell Faculty Career Initiation Grant.

REFERENCES

Alkhalifah, T., and Tsvankin, I., 1995, Velocity analysis in transversely isotropic media: Geophysics, **60**, 1550–1566.
Contreras, P., Grechka, V., and Tsvankin, I., 1999, Moveout inversion of P-wave data for horizontal transverse isotropy: Geophysics, **64**, 1219–1229.
Dellinger, J., and Muir, F., 1988, Imaging reflections in elliptically anisotropic media: Geophysics, **53**, 1616–1618.
Dix, C.H., 1955, Seismic velocities from surface measurements: Geophysics, **20**, 68–86.
Grechka, V., and Tsvankin, I., 1998, 3-D description of normal moveout in anisotropic inhomogeneous media: Geophysics, **63**, 1079–1092.
——— 1999, 3-D moveout velocity analysis and parameter estimation for orthorhombic media: Geophysics, **64**, 820–837.
Grechka, V., Tsvankin, I., and Cohen, J. K., 1999, Generalized Dix equation and analytic treatment of normal-moveout velocity for anisotropic media: Geophys. Prosp., **47**, 117–148.
Leslie, J. M., and Lawton, D. C., 1996, Structural imaging below dipping anisotropic layers: Predictions from seismic modeling: 66th Ann. Internat. Mtg., Soc. Expl. Geophys., Expanded Abstracts, 719–722.
Levin, F. K., 1971, Apparent velocity from dipping interface reflections: Geophysics, **36**, 510–516.
Sayers, C. M., and Ebrom, D. A., 1997, Seismic traveltime analysis for azimuthally anisotropic media: Theory and experiment: Geophysics, **36**, 1570–1582.
Taner, M. T., and Koehler, F., 1969, Velocity spectra–digital computer derivation and application of velocity functions: Geophysics, **34**, 859–881.
Thomsen, L., 1986, Weak elastic anisotropy: Geophysics, **51**, 1954–1966.
——— 1988, Reflection seismology over azimuthally anisotropic media: Geophysics, **53**, 304–313.
Tsvankin, I., 1995, Normal moveout from dipping reflectors in anisotropic media: Geophysics, **60**, 268–284.
——— 1996, P-wave signatures and notation for transversely isotropic media: An overview: Geophysics, **61**, 467–483.
——— 1997a, Reflection moveout and parameter estimation for horizontal transverse isotropy: Geophysics, **62**, 614–629.
——— 1997b, Moveout analysis for transversely isotropic media with a tilted symmetry axis: Geophys. Prosp., **45**, 479–512.
Tsvankin, I., and Thomsen, L., 1994, Nonhyperbolic reflection moveout in anisotropic media: Geophysics, **59**, 1290–1304.
——— 1995, Inversion of reflection traveltimes for transverse isotropy: Geophysics, **60**, 1095–1107.
Uren, N. F., Gardner, G. N. F., and McDonald, J. A., 1990, Normal moveout in anisotropic media: Geophysics, **55**, 1634–1636.
Vestrum, R. W., Lawton, D. C., and Schmid, R., 1999, Imaging structures below dipping TI media: Geophysics, **64**, 1239–1246.

APPENDIX A

NMO VELOCITY IN TTI MEDIA: SPECIAL CASES

NMO for steep reflectors

Generation of a specular zero-offset reflection requires that some portion of the incident wavefront be parallel to the reflecting interface [i.e., the phase-velocity (or slowness) vector for this segment must be orthogonal to the reflector]. If the medium above the reflector is homogeneous and has a horizontal plane of mirror symmetry, the wavefront of the downgoing wave contains the full range of phase angles. In other words, as the ray tilts away from the surface, the wavefront normal rotates from horizontal (for horizontal rays) to vertical and back to horizontal. As a result, specular reflections in a homogeneous layer with a horizontal symmetry plane (such as VTI or HTI) exist for the whole range of dips from 0° to 90° (Tsvankin, 1997b).

A tilt of the symmetry axis, however, makes the wavefront asymmetric with respect to horizontal, and its cross-sections in some azimuthal directions may contain only a limited range of phase angles. Tsvankin (1997b) studied the existence of specular reflections for the 2-D TTI model with the symmetry axis confined to the dip plane of the reflector. As illustrated in Figure A-1, if the symmetry axis is tilted toward the reflector, the maximum phase angle in the segment of the wavefront approaching the reflector ($\theta_{\max}$) typically is $<90^\circ$. Steep interfaces with the dip $\phi > \theta_{\max}$ reflect all incident rays downward and therefore become invisible on surface seismic data. If the medium is heterogeneous and velocity increases with depth, the missing dips may produce reflected arrivals at the surface, but these reflections represent turning rays. In contrast, for the symmetry axis tilted away from the reflector, it is possible to record reflections in homogeneous media even from overhang structures with dips exceeding 90° (Tsvankin, 1997b).

Here, we treat a more general situation of the symmetry axis making an arbitrary azimuth with the dip plane of the reflector.

Figure A-2 shows the maximum dip that generates a zero-offset reflected ray as a function of the azimuth of the symmetry axis for a particular TTI model. For the maximum dip, the zero-offset ray is horizontal and the NMO velocity in the ray direction is infinite, which means that the NMO ellipse degenerates into two parallel straight lines (Grechka and Tsvankin, 1998).

If the symmetry axis is confined to the dip plane and points toward the reflector ($\beta = 0$), the maximum dip for the model with $\nu = 25^\circ$, $\epsilon = 0.25$, and $\delta = 0.05$ is just 76° (Figure A-2b), which agrees with the result of Tsvankin (1997b, Figure 3). As the symmetry axis deviates from the dip plane, the range of missing dips becomes more narrow and vanishes altogether for $\beta = 90^\circ$, when the horizontal projection of the symmetry axis coincides with the reflector strike. For azimuth β larger than 90°, the maximum dip exceeds 90°, so it is possible to record surface reflections from overhang structures. If the symmetry axis is back in the dip plane but tilted away from the reflector ($\beta = 180^\circ$), the maximum dip may be >100° (Figures A-2b,c).

As discussed by Tsvankin (1997b), it does not take a large tilt of the symmetry axis for the maximum dip to deviate considerably from 90°. Because of the asymmetric shape of the P-wavefront with respect to 45°, the smallest maximum dip usually corresponds to tilt angles of 20° to 35° (Figure A-2). The results displayed in Figure A-2 also show that for typical TI models, the maximum dip is more sensitive to the parameter ϵ than it is to δ.

Elliptical anisotropy

A TI model with any orientation of the symmetry axis becomes elliptically anisotropic if $\epsilon = \delta$. For elliptical anisotropy, the P-wave slowness surface and wavefront (group-velocity surface) have an ellipsoidal shape, while the SV-wave velocity is equal to V_{S0} in all directions (i.e., is independent of angle).

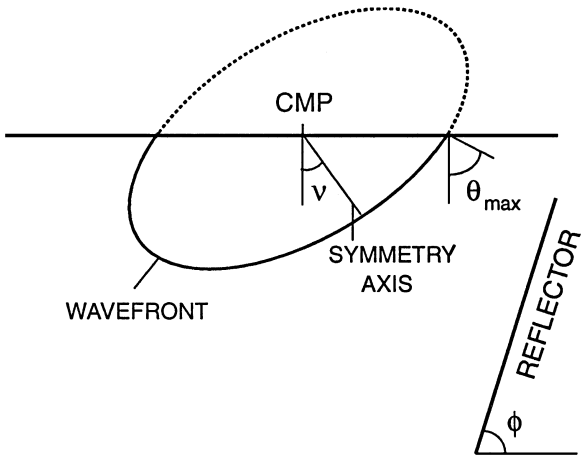

FIG. A-1. The P-wavefront for a TI medium with a symmetry axis tilted toward the reflector. The increase in phase and group velocity away from the symmetry axis in this model reduces the angular range of the wavefront normals in the segment of the wavefront propagating toward the reflector. The maximum phase (wavefront) angle in the lower-right quadrant is $\theta_{max} < 90^\circ$. Note that the maximum phase angle in the lower-left quadrant (not marked) exceeds 90° (after Tsvankin, 1997b).

Although the condition $\epsilon = \delta$ is seldom satisfied for subsurface formations (Thomsen, 1986), elliptical models require a special treatment in the inversion procedure and therefore must be considered separately.

Tsvankin (1997b) showed that for elliptical anisotropy the dip dependence of NMO velocity, expressed through the ray parameter p of the zero-offset ray, is exactly the same as in isotropic media:

$$V_{\rm nmo}(p) = \frac{V_{\rm nmo}(0)}{\sqrt{1 - p^2\, V_{\rm nmo}^2(0)}}, \qquad \text{(A-1)}$$

where $V_{\rm nmo}(0)$ corresponds to a horizontal reflector. This result, however, is limited to the dip plane of the reflector, under the assumption that this plane contains the symmetry axis of the medium.

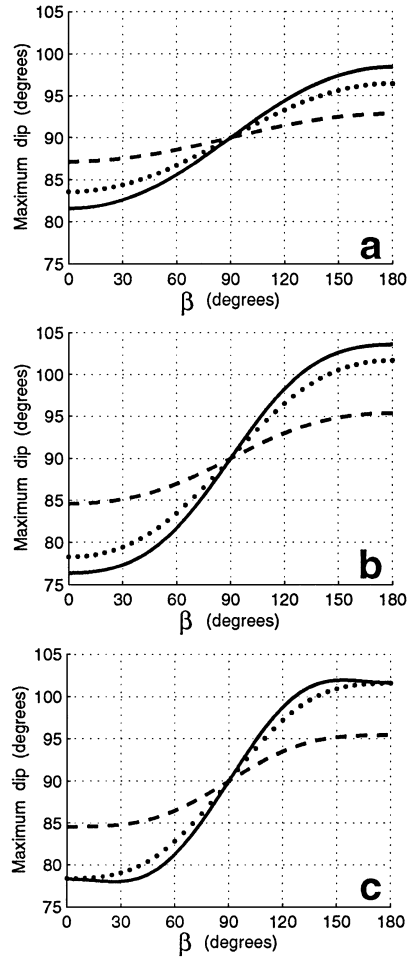

FIG. A-2. The dip of the steepest reflector that generates a zero-offset P-wave reflection in a homogeneous TTI layer. β is the azimuth of the symmetry axis with respect to the dip plane of the reflector. For $\beta = 0^\circ$, the symmetry axis points toward the reflector; for $\beta = 180^\circ$, it is tilted away from the reflector. Each plot corresponds to a different tilt of the symmetry axis: (a) $\nu = 10^\circ$; (b) $\nu = 25^\circ$; (c) $\nu = 40^\circ$. The solid curves are computed for $\epsilon = 0.25$ and $\delta = 0.05$; dotted for $\epsilon = 0.25$ and $\delta = 0.15$; dashed are for $\epsilon = 0.10$ and $\delta = 0.05$.

Analysis of equation (5) shows that in elliptical media the dependence of the P-wave NMO velocity on p_1 and p_2 remains isotropic for arbitrary orientations of the symmetry axis and reflector normal and any azimuth of the CMP line. The P-wave phase-velocity function for elliptical anisotropy is given by

$$V_P(\theta) = V_{P0}\sqrt{1 + 2\delta \sin^2\theta}, \tag{A-2}$$

where θ is the angle between the phase-velocity (slowness) vector and the symmetry axis. Representing θ through the slowness vector $\mathbf{p} = \{p_1, p_2, q\}$ and the symmetry axis orientation (defined by the unit vector $\mathbf{a}$ or the angles ν and β) yields

$$\cos\theta = V_P\,(\mathbf{p}\cdot\mathbf{a}) = V_P(p_1 \sin\nu\cos\beta + p_2 \sin\nu \sin\beta + q\cos\nu). \tag{A-3}$$

Combining equations (A-2) and (A-3) and taking into account that $V_P^2 = (p_1^2 + p_2^2 + q^2)^{-1}$ leads to a quadratic equation for q as a function of p_1 and p_2. Substituting $q(p_1, p_2)$ into equation (5), we find the following equation for the matrix $\mathbf{W}$ in elliptically anisotropic media:

$$W_{ij}(p_1, p_2) = W_{ij}(0, 0) - p_i p_j. \tag{A-4}$$

It is easy to verify that equation (A-4) is identical to the dependence of W_{ij} on p_1 and p_2 for isotropic media. Hence, the influence of elliptical anisotropy on NMO velocity in equation (A-4) is hidden in the NMO ellipse for horizontal events $[W_{ij}(0, 0)]$. This result has serious implications for the inversion procedure discussed in the main text. Equation (A-4), as any other isotropic kinematic relationship, can be also used for SV-waves in elliptical media.

The isotropic form of the function $W_{ij}(p_1, p_2)$ also means that conventional dip-moveout (DMO) algorithms developed for isotropic media are valid for elliptical anisotropy with any symmetry axis orientation. Since reflection moveout in elliptical media is purely hyperbolic (Uren et al., 1990), the diffraction curve on the zero-offset section (i.e., in the poststack domain) also has the same shape as in isotropic media. Hence, the poststack time-migration impulse response for elliptical anisotropy can be computed with isotropic algorithms using the correct (anisotropic) NMO velocity in any given azimuth. Still, if the symmetry axis is tilted, both the NMO velocity and migration impulse response in elliptical media vary with azimuth, which should be taken into account in the moveout correction and time migration. Dellinger and Muir (1988) describe a sequence of stretching operations that can be applied to velocity surfaces to correct for elliptical anisotropy in seismic imaging. The above conclusions, as well as equation (A-4), always apply to SH-waves because their propagation in any TI medium is governed by the elliptical dependencies.

TI layer with the symmetry axis perpendicular to the reflector

If TI layers (e.g., shales) were tilted because of tectonic processes after sedimentation, the symmetry axis remains perpendicular to the layering. The relative simplicity of this model makes it possible to obtain concise exact representation of the NMO ellipse for the reflection from the bottom of the tilted TI formation.

Since the dip plane of the reflector contains the symmetry axis, it becomes a vertical symmetry plane for the whole model and determines the orientation of the NMO ellipse. The semiaxis of the NMO ellipse that lies in the dip plane (the dip component of the NMO velocity denoted as $V_{\rm nmo}^{(1)}$) is given by (Tsvankin, 1995)

$$V_{\rm nmo}^{(1)}(\phi) = \frac{V_{\rm nmo}(0)}{\cos\phi}. \tag{A-5}$$

Here, ϕ is the reflector dip and $V_{\rm nmo}(0)$ is the NMO velocity from a horizontal interface obtained under the assumption that the symmetry axis is perpendicular to the reflector (i.e., it is vertical for a horizontal reflector). Equation (A-5) is identical to the cosine-of-dip dependence of NMO velocity in isotropic media (Levin, 1971), with $V_{\rm nmo}(0)$ replacing the medium velocity.

Introducing the ray parameter $p = \sqrt{p_1^2 + p_2^2}$ into equation (A-5), we obtain

$$V_{\rm nmo}^{(1)}(p) = \frac{V_{\rm nmo}(0)}{\sqrt{1 - p^2 V_0^2}}, \tag{A-6}$$

where $V_0 = \sin\phi/p$ is the symmetry-direction velocity of the mode under consideration (it can be either a P- or an S-wave). Since in anisotropic media $V_{\rm nmo}(0)$ and V_0 generally are different, equation (A-6) does not coincide with the corresponding isotropic expression.

Next, it is interesting to examine whether the strike component of the NMO velocity $V_{\rm nmo}^{(2)}$ provides any additional information about the medium. Straightforward but tedious algebraic transformations of equation (5) give

$$V_{\rm nmo}^{(2)} = V_{\rm nmo}(0). \tag{A-7}$$

For P-waves this result can be obtained more easily in the weak-anisotropy approximation (discussed in detail in Appendix B) by substituting the relation $\tan\nu = \tan\phi = p_1/p_3$ into equation (B-7) for W_{22}. Therefore, $V_{\rm nmo}^{(2)}$ is equal to the zero-dip NMO velocity and is completely independent of dip, comparable to the result of Levin (1971) for isotropic media.

Combining the two semiaxes of the NMO ellipse [equations (A-6) and (A-7)] and obtaining p from the zero-offset section, we can find $V_{\rm nmo}(0)$ and the symmetry-direction velocity V_0. Since for the P-wave $V_{\rm nmo}(0) = V_{P0}\sqrt{1 + 2\delta}$ [equation (1)], the P-wave NMO ellipse for a dipping event yields the anisotropic parameter δ in addition to the symmetry-direction velocity V_{P0}. [Likewise, the NMO ellipse of the SV-wave provides the symmetry-direction velocity V_{S0} and the anisotropic parameter $\sigma = (V_{P0}^2/V_{S0}^2)(\epsilon - \delta)$.] Then equation (A-5) can be used to find the tilt ν equal to the reflector dip ϕ.

Both $V_{\rm nmo}(0)$ and δ can be determined even from 2-D P-wave data acquired in the dip plane if the zero-dip velocity $V_{\rm nmo}(0)$ was found from a horizontal event. Note that $V_{\rm nmo}(0)$ corresponds to a horizontal reflector and a vertical symmetry axis; we can imagine, for instance, that the reflecting interface may have a gradually changing slope, with the symmetry axis remaining orthogonal to the reflector. According to Leslie and Lawton (1996), such a model is typical for the Canadian Foothills.

APPENDIX B

P-WAVE NMO ELLIPSE IN A WEAKLY ANISOTROPIC TTI LAYER

The matrix **W** [equation (5)] that determines the NMO ellipse can be linearized with respect to the anisotropic coefficients ϵ and δ under the assumption of weak anisotropy ($|\epsilon| \ll 1$ and $|\delta| \ll 1$). Without losing generality, we assume that the symmetry axis (unit vector **a**) lies within the coordinate plane $[x_1, x_3]$ (Figure B-1). Then

$$\mathbf{a} \equiv [a_1, 0, a_3] = [\sin\nu, 0, \cos\nu], \tag{B-1}$$

where ν is the tilt of the axis.

To obtain the elements of the matrix **W**, we need to solve the Christoffel equation for the vertical component of the slowness vector $q \equiv p_3$ as a function of the horizontal slowness components p_1 and p_2. The Christoffel equation for TI media can be written as

$$\begin{aligned} F \equiv &\left(c_{11}s^2 + c_{44}c^2 - 1\right)\left(c_{44}s^2 + c_{33}c^2 - 1\right) \\ &- (c_{13} + c_{44})^2 s^2 c^2 = 0, \end{aligned} \tag{B-2}$$

where $s = |\mathbf{p}|\sin\theta$ and $c = |\mathbf{p}|\cos\theta$; and where θ is the angle between the slowness vector **p** and the symmetry axis **a**. Expressing s and c through the components of the vectors **p** and **a**, we find

$$s^2 \equiv [\mathbf{a}\times\mathbf{p}]\cdot[\mathbf{a}\times\mathbf{p}] = p_2^2 + (a_3 p_1 - a_1 q)^2$$

and

$$c^2 \equiv (\mathbf{a}\cdot\mathbf{p})^2 = (a_1 p_1 + a_3 q)^2.$$

Next, we replace the stiffness coefficients c_{ij} with Thomsen (1986) parameters defined with respect to the symmetry axis:

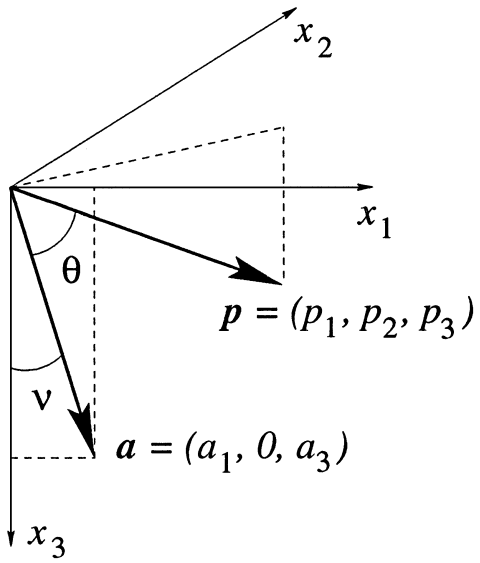

FIG. B-1. In the derivation of the weak anisotropy approximation, the symmetry axis (described by the unit vector **a**) is assumed to be confined to the $[x_1, x_3]$-plane. The value **p** is the slowness vector.

$$\begin{aligned} &c_{33} = \rho V_{P0}^2, \quad c_{44} = \rho V_{S0}^2, \quad c_{11} = \rho V_{P0}^2(1 + 2\epsilon), \\ &c_{13} = \rho\sqrt{\left(V_{P0}^2 - V_{S0}^2\right)\left(V_{P0}^2(1 + 2\delta) - V_{S0}^2\right)} - \rho V_{S0}^2, \end{aligned} \tag{B-3}$$

where ρ is the density.

The linearized solution of the Christoffel equation (B-2) for the vertical slowness q can be represented as the sum of the isotropic value $\tilde{q}$ and the correction term Δq resulting from the influence of anisotropy:

$$q \equiv p_3 = \tilde{q} + \Delta q. \tag{B-4}$$

For *P*-waves, the vertical slowness in isotropic media is given by

$$\tilde{q} = \sqrt{\frac{1}{V_{P0}^2} - p_1^2 - p_2^2}. \tag{B-5}$$

The value Δq can be considered as the linear term in a Taylor series expansion of q in ϵ and δ for fixed horizontal slownesses p_1 and p_2:

$$\Delta q = -\frac{1}{\partial F/\partial p_3}\left(\frac{\partial F}{\partial \epsilon}\,\epsilon + \frac{\partial F}{\partial \delta}\,\delta\right), \tag{B-6}$$

with the partial derivatives obtained by differentiating the Christoffel equation $F = 0$ (B-2). Combining equations (B-4), (B-5), and (B-6) yields q as a function of p_1 and p_2 in weakly anisotropic TTI media.

Now we can obtain the derivatives $q_{,i} = \partial q/\partial p_i$ and $q_{,ij} = \partial^2 q/\partial p_i \partial p_j$, $(i, j = 1, 2)$ from equation (B-4) and substitute them into the exact equation (5) for the matrix **W**. Further linearization of **W** in the anisotropic parameters using symbolic software Mathematica leads to the following result:

$$\begin{aligned} W_{11} = &\frac{1}{V_{P0}^2}\left(1 - 2\delta + 2\epsilon a_1^2 - 14(\epsilon - \delta)a_1^2 a_3^2\right) \\ &- p_1^2 + \hat{W}_{11}(\epsilon - \delta), \end{aligned} \tag{B-7}$$

$$W_{12} = -p_1 p_2 + \hat{W}_{12}(\epsilon - \delta),$$

and

$$W_{22} = \frac{1}{V_{P0}^2}\left(1 - 2\delta - 2(\epsilon - \delta)a_1^2\left(1 + a_3^2\right)\right) - p_2^2 + \hat{W}_{22}(\epsilon - \delta).$$

In equations (B-7), $y_1 = p_1^2 V_{P0}^2$, $y_2 = p_2^2 V_{P0}^2$,

$$\begin{aligned} \hat{W}_{11} = &\, 2p_1^2\left(-6 + 9y_1 - 4y_1^2\right)\left(1 - 8a_1^2 a_3^2\right) \\ &+ 8a_1 a_3 p_1 \tilde{q}\left(1 - 2a_1^2\right)\left(3 - 7y_1 + 4y_1^2\right) \\ &+ 2p_2^4 a_3^4 V_{P0}^2(1 - 4y_1) \\ &+ 4p_2^2\left[a_3^2\left(1 - 4a_1^2\right)\left(-1 + 5y_1 + 4y_1^2\right)\right. \\ &\left.+ 2a_1 a_3^3 p_1 \tilde{q} V_{P0}^2(-3 + 4y_1)\right], \end{aligned}$$

$$\hat{W}_{12} = 8p_1p_2\big[-y_2^2a_3^4 + y_2a_3^2\big(2-5a_1^2-2y_1\big(1-4a_1^2\big)\big) - a_3^2\big(1-4a_1^2\big) + y_1\big(2-a_1^2-12a_1^2a_3^2\big) - y_1^2\big(1-8a_1^2a_3^2\big)\big] + 8a_1a_3p_2\tilde{q}\big[a_3^2\big(1-y_2\big(1-4y_1\big)\big) - y_1\big(5-8a_1^2\big) + 4y_1^2\big(1-2a_1^2\big)\big],$$

and

$$\hat{W}_{22} = -4p_1^2a_3^2\big(1-4a_1^2\big) + 2p_1^2y_1 - 16p_1^2y_1a_1^2a_3^2 + 8a_1a_3p_1\tilde{q}\big[a_3^2 - y_1\big(1-2a_1^2\big) - y_2\big(5a_1^2-4y_1\big(1-2a_1^2\big)\big)\big] + 4p_2^2\big[-3a_3^4+5y_1a_3^2\big(1-4a_1^2\big)-2y_1^2\big(1-8a_1^2a_3^2\big)\big] + 2p_2^2y_2a_3^2\big[9a_3^2-8y_1\big(1-4a_1^2\big) + 16a_1a_3p_1\tilde{q}V_{P0}^2\big] - 8p_2^2y_2^2a_3^4. \quad \text{(B-8)}$$

APPENDIX C

JOINT INVERSION OF *P*- AND *SV*-WAVE MOVEOUT IN A TTI LAYER

P- and *SV*-wave propagation in TI media is controlled by the same set of the stiffness coefficients c_{ij}. If the stiffnesses are replaced with Thomsen parameters, *P*-wave kinematics becomes practically independent of the shear-wave symmetry-direction velocity V_{S0}, but both *P*- and *SV*-wave velocities are still influenced by V_{P0}, ϵ, δ, and the orientation of the symmetry axis. Hence, we can expect to increase the stability of the inversion procedure discussed in the main text by combining *P*-wave data with *SV*-wave NMO ellipses.

In this appendix, we modify our parameter-estimation algorithm by adding the NMO velocity of *SV*-waves from a horizontal reflector to the input data. The *SV*-wave NMO ellipse for horizontal events in the weak-anisotropy approximation can be obtained from the corresponding *P*-wave equations (6)–(8) by making the following parameter substitutions (Tsvankin, 1995, 1997b): the velocity V_{P0} should be replaced with V_{S0}, ϵ set to zero, and δ replaced with the parameter σ defined as

$$\sigma \equiv \left(\frac{V_{P0}}{V_{S0}}\right)^2 (\epsilon - \delta). \quad \text{(C-1)}$$

This yields the following expressions for the semiaxes of the *SV*-wave ellipse from a horizontal reflector (the axis x_1 is parallel to the horizontal projection of the symmetry axis):

$$V_{\mathrm{nmo},SV}^{(1)}(0) = V_{S0}\sqrt{1+2\sigma\,(1-7\sin^2\nu\cos^2\nu)} \quad \text{(C-2)}$$

and

$$V_{\mathrm{nmo},SV}^{(2)}(0) = V_{S0}\sqrt{1+2\sigma\,\cos^4\nu}. \quad \text{(C-3)}$$

For VTI media ($\nu = 0$), equations (C-2) and (C-3) reduce to the azimuthally independent *SV*-wave NMO velocity given by Thomsen (1986),

$$V_{\mathrm{nmo},SV}(0) = V_{S0}\sqrt{1+2\sigma}. \quad \text{(C-4)}$$

The *SV*-wave NMO ellipse degenerates into a circle not only for VTI media but also if the above trigonometric functions multiplied with 2σ are identical, i.e., $\cos^2\nu = 1/6$ ($\nu = 65.9^\circ$). For a tilt of 65.9°, the *P*-wave NMO ellipse can also become a circle, but only if $\epsilon = 0$ [see equation (11)].

The NMO velocities of *P*- and *SV*-waves in a horizontal VTI layer are insufficient to determine the vertical velocities and anisotropic coefficients (Tsvankin and Thomsen, 1995). Although the vertical-velocity ratio V_{P0}/V_{S0} can be found from the zero-offset traveltimes, the two NMO velocities still contain three unknown parameters (V_{P0}, δ, and σ or ϵ). The only exception is elliptical anisotropy, for which the *SV*-wave velocity is independent of angle and the NMO velocity is equal to V_{S0}. Then V_{P0} can be found from the zero-offset traveltimes, and the *P*-wave NMO velocity yields the anisotropic parameter $\epsilon = \delta$. This inversion procedure, however, is based on the assumption that the medium is elliptical, which cannot be verified from the data unless dipping events or long-spread moveout are available.

If the symmetry axis is tilted, we can take advantage of the azimuthal dependence of NMO velocity. The NMO ellipses of *P*- and *SV*-waves in a horizontal TTI layer provide six equations for the medium parameters, five of which are independent (the two ellipses have the same orientation determined by the azimuth of the symmetry axis). In principle, the number of equations can go down to four if both ellipses degenerate into circles, but the above analysis shows that this situation is highly unlikely. (For weak anisotropy, both ellipses become circles only if the conditions $\cos^2\nu = 1/6$ and $\epsilon = 0$ are satisfied simultaneously.) Including *SV*-waves also allows us to obtain the ratio of the zero-offset traveltimes $r = t_{P0}/t_{SV0}$ and add a sixth equation into the inversion procedure.

Thus, combining *P*- and *SV*-data in a horizontal TTI layer results in a system of six nonlinear equations for six unknowns (V_{P0}, V_{S0}, ϵ, δ, ν, and β). Unfortunately, numerical analysis of this system shows that it does not have a unique solution. As illustrated by Figure C-1, it is possible to find at least two different realistic TTI models that yield practically identical NMO ellipses of *P*- and *SV*-waves. Also, the ratio of the zero-offset traveltimes for both models from Figure C-1 is the same ($r = 0.546$).

Since the *P*- and *SV*-wave NMO ellipses from a horizontal reflector do not provide enough information for unambiguous parameter estimation, we add the *P*-wave NMO velocity for a dipping event to the input data and construct the following objective function:

$$\mathcal{F}_{P,SV} = \left(\frac{r}{\tilde{r}}-1\right)^2 + \int_0^{2\pi}\left[1-\frac{V_{\mathrm{nmo},P}^{\mathrm{hor}}(\alpha)}{\tilde{V}_{\mathrm{nmo},P}^{\mathrm{hor}}(\alpha)}\right]^2 d\alpha + \int_0^{2\pi}\left[1-\frac{V_{\mathrm{nmo},P}^{\mathrm{dip}}(\alpha)}{\tilde{V}_{\mathrm{nmo},P}^{\mathrm{dip}}(\alpha)}\right]^2 d\alpha + \int_0^{2\pi}\left[1-\frac{V_{\mathrm{nmo},SV}^{\mathrm{hor}}(\alpha)}{\tilde{V}_{\mathrm{nmo},SV}^{\mathrm{hor}}(\alpha)}\right]^2 d\alpha. \quad \text{(C-5)}$$

As in equation (13), $\tilde{V}_{\mathrm{nmo}}$ denotes the NMO velocities measured from the data, while V_{nmo} is calculated from the exact equation (5).

Compared to the pure P-wave inversion in the previous section, the objective function contains three more equations and only one additional unknown parameter (V_{S0}), which helps to stabilize the inversion procedure. Overall, the joint inversion of P- and SV-data involves solving nine nonlinear equations (provided that none of the ellipses degenerates into a circle) for six unknowns: V_{P0}, V_{S0}, ϵ, δ, ν, and β.

Typical results of parameter estimation for a TTI layer obtained by minimizing the objective function (C-5) are presented in Figure C-2. As in the P-wave inversion, we added Gaussian noise with a variance of 2% to all NMO ellipses and performed the inversion 200 times for different realizations of the input data. Figure C-2 exhibits the same general trend as that for the P-wave results in Figure 2: the inversion procedure becomes more stable with increasing tilt ν of the symmetry axis. Comparison of the corresponding plots in Figures 2 and C-2 shows, however, that the scatter in the inverted values is higher for the pure P-wave inversion (Figure 2), especially for tilts of 20° and 40°. Therefore, as expected, the addition of the SV-wave NMO ellipse from a horizontal reflector to P-wave data increases the stability of parameter estimation.

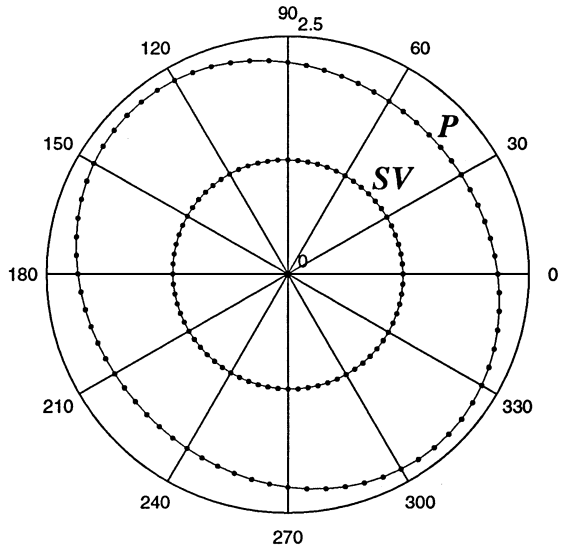

FIG. C-1. NMO ellipses of P- and SV-waves calculated from equation (5) in a horizontal TTI layer for two different sets of medium parameters. The parameters used to compute the solid ellipses are $V_{P0} = 2.0$ km/s, $V_{S0} = 1.2$ km/s, $\epsilon = 0.2$, $\delta = 0.1$, and $\nu = 60°$. For the dotted ellipses, $V_{P0} = 1.902$ km/s, $V_{S0} = 1.204$ km/s, $\epsilon = 0.273$, $\delta = 0.253$, and $\nu = 49.7°$. The azimuth of the symmetry axis $\beta = 40°$ is the same for both models.

Nonetheless, even the combination of P- and SV-data is not sufficient to resolve all medium parameters in a stable fashion if the tilt of the symmetry axis is small (Figure C-2a–c). In principle, in the limit of $\nu = 0$ (VTI media) we can find ϵ, δ, and the symmetry direction (vertical) velocities separately because, after obtaining $\eta \approx \epsilon - \delta$ from the dip dependence of P-wave NMO velocity and the V_{P0}/V_{S0} ratio from the vertical traveltimes, we can determine V_{S0} (and then all other parameters) using the SV-wave velocity for a horizontal event [equation (C-4)]. However, while this inversion works well on noise-free data, small errors in η propagate with significant amplification into the value of σ [equation (C-1)] and the vertical velocities. Hence, despite the parameter η being well resolved (Figure C-2a), we observe an increased scatter in V_{P0}, V_{S0}, ϵ, and δ for mild tilt angles.

The addition of the SV-wave NMO ellipse for a horizontal reflector does help, however, to overcome the ambiguity of P-wave inversion for elliptical anisotropy. In this case, the dip dependence of the P-wave NMO ellipse is sufficient only to establish the fact that $\epsilon = \delta$, and the parameters V_{P0}, ϵ, ν, and β cannot be found from a single P-wave NMO ellipse for a horizontal event. The SV-wave phase velocity in elliptical media is independent of angle, so the NMO velocity from a horizontal reflector is equal to V_{S0} in any direction. After obtaining V_{S0} from the SV-wave moveout, we can use the ratio of the zero-offset P and SV traveltimes as an additional equation, which allows us to resolve all medium parameters. Our numerical analysis shows that this inversion procedure is reasonably stable.

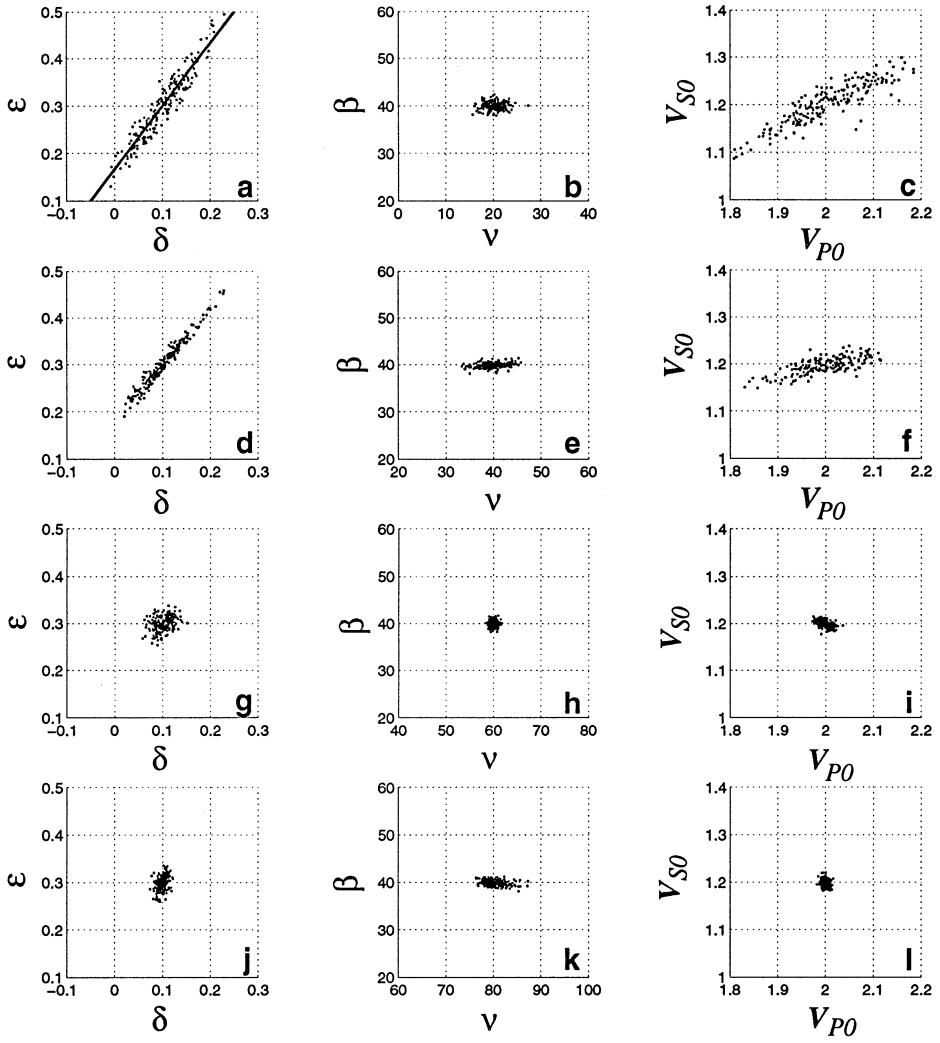

FIG. C-2. Inverted values of the parameters ϵ, δ, β, ν, V_{P0}, and V_{S0} in a homogeneous TTI layer. For input data, we use the P-wave NMO ellipses from a horizontal and a dipping reflector (dip $\phi = 60^\circ$, azimuth $= 50^\circ$, the same as in Figure 2), the SV-wave NMO ellipse from a horizontal reflector, and the ratio of the zero-offset traveltimes of P- and SV-waves. All NMO ellipses were distorted by random noise with a variance of 2%. The medium parameters are the same as in Figure 2: $V_{P0} = 2.0$ km/s, $V_{S0} = 1.2$ km/s, $\epsilon = 0.3$, $\delta = 0.1$, $\beta = 40^\circ$. The tilt ν is equal to 20° in (a), (b), and (c); 40° in (d), (e), and (f); 60° in (g), (h), and (i); and 80° in (j), (k), and (l). The solid line on plot (a) corresponds to the correct value of $\eta = 0.167$.